Thymic dendritic cell-derived IL-27p28 promotes the establishment of functional bias against IFN-γ production in newly generated CD4^{+} T cells through STAT1-related epigenetic mechanisms

Jie Zhang[1], Hui Tang[1], Haoming Wu[1], Xuewen Pang[1], Rong Jin[1*], Yu Zhang[1,2*]

[1] Department of Immunology, School of Basic Medical Sciences, NHC Key Laboratory of Medical Immunology, Medicine Innovation Center for Fundamental Research on Major Immunology-related Diseases, Peking University, Beijing, China

2 Institute of Life Sciences, Jinzhou Medical University, Jinzhou, Liaoning Province, China

Corresponding Author

Yu Zhang, zhangyu007@bjmu.edu.cn

Rong Jin, jinrong@bjmu.edu.cn

Keywords: IL-27p28, single positive thymocyte, Th2 bias, IFN-γ, autoimmune disease

Abstract

The newly generated CD4 single-positive (SP) T lymphocytes are featured by enhanced IL-4 but repressed IFN-γ production. The mechanisms underlying this functional bias remain elusive. Previous studies have reported that $CD4^+$ T cells from mice harboring DC-specific deletion of IL-27p28 display an increased capacity of IFN-γ production upon TCR stimulation. Here we demonstrated that similarly altered functionality occurred in CD4SP thymocytes, recent thymic emigrants (RTEs) as well as naive T cells from either *Cd11c-p28*$^{f/f}$ mice or mice deficient in the α subunit of IL-27 receptor. Therefore, DC-derived IL-27p28-triggered, IL-27Rα-mediated signal is critically involved in the establishment of functional bias against IFN-γ production during their development in the thymus. Epigenetic analyses indicated reduced DNA methylation of the *Ifng* locus and increased trimethylation of H3K4 at both *Ifng* and *Tbx21* loci in CD4SP thymcoytes from *Cd11c-p28*$^{f/f}$ mice. Transcriptome profiling demonstrated that *Il27p28* ablation resulted in coordinated up-regulation of STAT1-activated genes. Concurrently, STAT1 was found to be constitutively activated. Moreover, we observed increased accumulation of STAT1 at the *Ifng* and *Tbx21* loci and a strong correlation between STAT1 binding and H3K4me3 modification of these loci. Of note, *Il27p28* deficiency exacerbated the autoimmune phenotype of *Aire*$^{-/-}$ mice. Collectively, this study reveals a novel mechanism underlying the functional bias of newly generated $CD4^+$ T cells and the potential relevance of such a bias in autoimmunity.

41 Graphic abstract

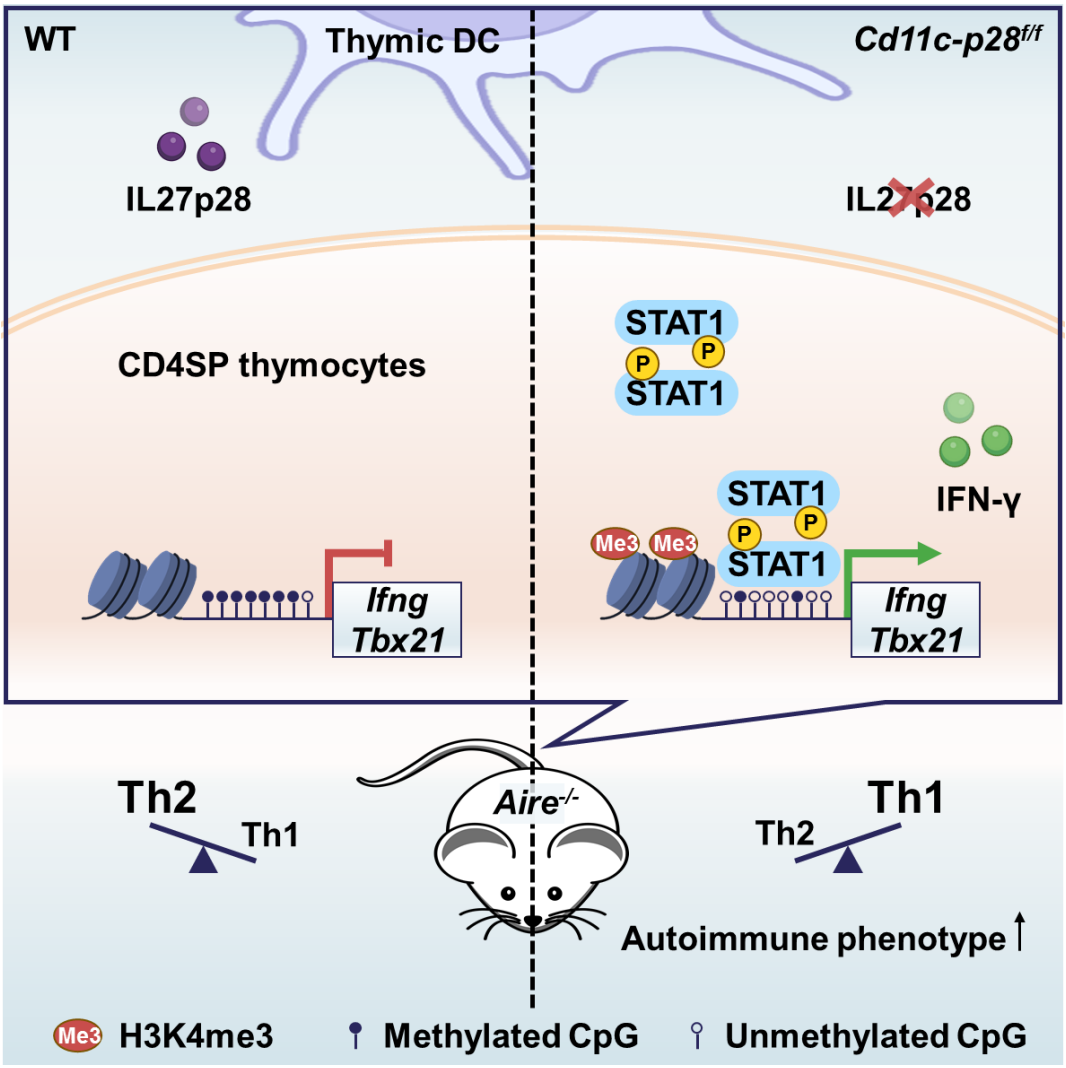

42

Introduction

The thymus plays a crucial role in the phenotypic development and functional maturation of T cells. After positive and negative selection, T cell progenitors become CD4 or CD8 single positive (CD4SP or CD8SP) thymocytes that are self-tolerant. These SP thymocytes then emigrate to the periphery, known as recent thymic emigrants (RTEs), and 2-3 weeks later, RTEs develop into mature naive T cells (*Ashby & Hogquist, 2023*). Upon activation, CD4SP thymocytes and RTEs exhibit a reduced proliferation capacity and decreased production of interleukin-2 (IL-2), interferon-γ (IFN-γ), and tumor necrosis factor α (TNF-α) compared to mature naive T cells. However, they show increased secretion of IL-4, which is known as T helper (Th) 2 bias in immature T cells (*Hendricks & Fink, 2011*). This Th2 bias in CD4SP thymocytes and RTEs is thought to assist newly emigrated self-reactive T cells to respond appropriately to self-antigens (*Fink & Hendricks, 2011*). Furthermore, the low level of IFN-γ production in RTEs renders them more prone to becoming regulatory T cells, which also helps to prevent the induction of autoimmune diseases (*Bhaumik et al., 2013*). The low level of DNA methylation at the *Il4* locus and reduced expression of *Dnmts* contribute to the Th2 bias in CD4SP thymocytes and RTEs (*Berkley et al., 2013*). However, the mechanism behind repressed IFN-γ expression in favor of the Th2 bias in these immature T cells is elusive.

The heterodimeric cytokine IL-27 is composed of IL-27p28 and Epstein-Barr virus-induced gene 3 (EBI3), which signals through the IL-27R consisting of the IL-27Rα (also named as WSX-1, TCCR) and the gp130 subunits. Elevated levels of IL-27 are associated with the pathogenesis of autoimmune diseases such as ankylosing

65 spondylitis (AS) (*Lin et al., 2015*), behcet's disease (BD) (*Shen et al., 2013*), and
66 experimental arthritis (*Cao et al., 2008*). The IL-27-regulated differentiation and
67 function of peripheral $CD4^+$ T cells subsets Th1, Th17 and Treg have been proposed as
68 an explanation for the pathogenesis of autoimmune disease (*Mei et al., 2021*), however,
69 conflicting reports have been demonstrated in different settings. For example, it is
70 consistent that IL-27 inhibits Th17 differentiation and function *in vitro* and *in vivo* in
71 *Il27p28*$^{-/-}$ and *Ebi3*$^{-/-}$ experimental autoimmune encephalomyelitis (EAE) mice models
72 (*Diveu et al., 2009; Kim et al., 2019; Liu et al., 2012*). Although IL-27 inhibits Treg
73 differentiation *in vitro* (*Huber et al., 2008; Neufert et al., 2007*), and *Ebi3*$^{-/-}$ EAE models
74 show increased numbers and suppressive functions of Tregs (*Liu et al., 2012*), Tregs in
75 *Il27ra*$^{-/-}$ and Treg-specific *Il27ra*$^{-/-}$ mice loss the suppressive function (*Kim et al., 2019;*
76 *Nguyen et al., 2019; Y. J. Park et al., 2019*). Furthermore, IL-27 was initially found to
77 promote Th1 differentiation of naive $CD4^+$ T cells under physiological conditions
78 (*Pflanz et al., 2002*). However, naive $CD4^+$ T cells derived from *Ebi3*$^{-/-}$ and *Il27p28*$^{-/-}$
79 mice exhibit increased production of IFN-γ. In addition, the absence of *Il27ra*$^{-/-}$
80 promotes pathological Th1 accumulation following *Trypanosoma cruzi* infection
81 (*Hamano et al., 2003; Pflanz et al., 2002; Villarino et al., 2003*). A subsequent study
82 demonstrates that both the absence and overexpression of IL-27p28 lead to increased
83 susceptibility to *T. gondii* infection, with IL-27p28 attributed as an independent
84 negative regulator of IFN-γ production in T cells (*J. Park et al., 2019*). Notably,
85 deficiency in gp130 does not alter IFN-γ production in $CD4^+$ T cells in a virus-infection
86 model (*Harker et al., 2015*). These results indicate the intricate functionality of each

87 subunit of IL-27 and IL 27R on peripheral $CD4^+$ T cells, which is insufficient to fully
88 explain the pathogenesis of autoimmune disease.

89 The structural analysis of IL-27 has demonstrated that IL-27p28, serving as a
90 central subunit, possesses the ability to bind with EBI3, as well as the two receptor
91 subunits IL-27Rα and gp130 (*Caveney et al., 2022*). Previous studies have reported IL-
92 27p28 as an independent antagonist of gp130-mediated signaling (*Stumhofer et al.,*
93 *2010*). In a ConA-induced liver damage model, $CD4^+$ T cells from mice with dendritic
94 cell (DC)-specific deletion of p28 (*Cd11c-p28*$^{f/f}$ mice) exhibit a propensity for rapid and
95 robust production of IFN-γ upon activation. This observation is attributed to the absence
96 of IL-27p28 in the thymic environment of these mice (*Zhang et al., 2013*). These
97 findings raise the intriguing possibility that thymic DC-derived IL-27p28 may
98 contribute to shaping the Th1/Th2 balance of newly generated CD4SP thymocytes.
99 In this paper, we have demonstrated that DC-derived IL-27p28 plays a crucial role in
100 maintaining the Th2 bias of CD4SP thymocytes. Our findings suggest that IL-27p28
101 regulates the DNA methylation status and histone modification of transcription
102 regulatory regions of *Ifng* and *Tbx21* genes. These epigenetic modifications were
103 further modulated by the low level of basal and phosphorylated signal transducer and
104 activator of transcription 1 (STAT1) protein. Furthermore, we observed that the
105 disruption of Th2 bias in CD4SP thymocytes due to IL-27p28 deficiency exacerbated
106 autoimmune diseases in *Aire*$^{-/-}$ mice. Our results provide insights into the molecular
107 mechanisms underlying the regulation of Th2 bias by DC-derived IL-27p28 and its
108 potential role in autoimmune diseases.

Results

1. DC-specific deletion of IL-27p28 endows the newly generated CD4$^+$ T cells with inherently enhanced capacity of IFN-γ production

Although IL-27 is widely reported to promote peripheral Th1 differentiation *in vitro*, CD4$^+$ T cells from *Cd11c-p28$^{f/f}$* mice exhibit enhanced IFN-γ production, a capacity seemingly acquired in their development in the thymus (*Zhang et al., 2013*). To investigate the possibility that thymic DC-derived IL-27 shapes the functionality of newly generated CD4$^+$ T cells, CD4SP thymocytes, CD4$^+$ RTEs, and CD4$^+$ naive T cells were purified from *Cd11c-p28$^{f/f}$* (cKO) mice and their wild-type (WT) littermates harboring a Rag2-GFP transgene, which allows easy tracking of newly generated thymocytes and RTEs (*Ashby & Hogquist, 2023*). The purified cells were then compared for cytokine expression in response to anti-CD3 and anti-CD28 stimulation under non-polarizing conditions. As expected, CD4$^+$ naive T cells from cKO mice exhibited a significantly higher level of *Ifng* mRNA expression compared to WT cells (Figure 1A). Intracellular staining (Figure 1B) and ELISA assay of the culture supernatant (Figure 1C) confirmed enhanced IFN-γ production at the protein level. Notably, this difference was already detectable at the SP thymocyte stage, indicating that it is developmentally regulated. Another prominent feature of CD4SP thymocytes is the hyperproduction of Th2 cytokines (*Fink & Hendricks, 2011; Makar et al., 2003*). Despite the profound impact of IL-27p28 deficiency on IFN-γ production, we observed no significant difference in IL-4 expression between cKO and WT T cells (Figure 1A and C). Moreover, there was no significant difference in the expression of IL-2 and

131 TNF-α between cKO and WT T cells (Figure 1A and Figure 1-figure supplement 1).
132 These results suggest that DC-specific deletion of IL-27p28 specifically enhances IFN-
133 γ production in newly generated T cells without affecting Th2 cytokines.

134 Next, we investigated the expression of T-box transcription factor (T-bet) and
135 GATA3, which are the master regulators of Th1 and Th2 differentiation, respectively
136 (*Fang et al., 2022*). The differential impact of IL-27p28 deficiency on IFN-γ and IL-4
137 production was accompanied by an increase in Tbx21 expression but no significant
138 alteration in Gata3 expression (Figure 1D). Western blotting confirmed the upregulation
139 of T-bet protein expression (Figure 1E). Furthermore, we extended our analyses onto
140 $CD4^+$ T cells at steady state or under polarizing conditions. Higher basal levels of *Ifng*
141 and *Tbx21* transcripts were detected in CD4SP thymocytes and naive T cells from cKO
142 mice than the counterparts from WT mice even without stimulation (Figure 1F),
143 indicating the constitutive activation of these loci. When cultured under polarizing
144 conditions, these cells were effectively induced to differentiate into Th1, Th2, Th17 and
145 Treg lineages. In contrast to the previous report of different differentiation potentials of
146 RTEs versus naive T cells (*Hendricks & Fink, 2011*), CD4SP thymocytes, RTEs and
147 naive T cells showed similar capacity to differentiate into effector cells. Moreover, cKO
148 and WT cells were equally positioned for the differentiation (Figure 1-figure
149 supplement 2A-F), suggesting that IL-27p28 deficiency does not affect effector cell
150 differentiation under optimal conditions. Taken together, these data support that IL-
151 27p28 is actively involved in the functional maturation of developing CD4SP
152 thymocytes, biasing them away from the Th1 lineage.

2. *Il27ra*-deficient CD4$^+$ T cells are similarly predisposed for potent IFN-γ production

Apart from acting as a subunit of IL-27, IL-27p28 have been reported to possess activities independent of IL-27, by acting on its own or coupling with other proteins, such as IL-Y (p28/p40, binding to IL-27Rα/IL-12Rβ1 to activate STAT3) (*Flores et al., 2015*) and CLY (p28/CLF, binding to gp130/IL-6Rα to activate STAT1 and STAT3) (*Tormo et al., 2013*). To ascertain whether the phenotype in the *Cd11c-p28$^{f/f}$* mice results from defective IL-27Rα signaling, we investigated the functional characters of T lineage cells in mice deficient in *Il27ra*. Reminiscent to what was observed in *Il27p28*-deficient mice, increased expression of *Ifng* and *Tbx21* were detected in *Il27ra$^{-/-}$* CD4SP thymocytes and naive CD4$^+$ T cells, whereas *Il4*, *Il2*, and *Gata3* transcripts were equally present in WT and *Il27ra$^{-/-}$* cells (Figure 2A). Intracellular staining confirmed the enhanced IFN-γ production by *Il27ra*-deficient cells stimulated under non-polarizing conditions (Figure 2B). IFN-γ production by *Il27ra$^{-/-}$* and WT cells, however, was comparable under Th1 polarizing conditions (Figure 1-figure supplement 2G). The similar phenotype shared by *Il27p28* and *Il27ra* knockout mice indicates that the altered T cell functionality in the absence of IL-27p28 is indeed a reflection of disrupted IL-27Rα signaling.

3. IL-27p28 deficiency induces permissive epigenetic changes at *Ifng* and *Tbx21* loci

Developmentally regulated transcriptional activation and repression of genes or cell-type specific expression patterns are largely achieved by modifying the chromatin template at a gene locus (*Ivashkiv, 2018*). Murine neonatal $CD4^+$ T cells have been documented to be poised to rapid Th2 cytokine secretion due to the pre-existing hypomethylation at a key Th2 cytokine regulatory region (*Rose et al., 2007*). In other reports, Th2 polarization in adult SP thymocytes and RTEs is attributable to active recruitment of DNA methyltransferases and increased H3K4 methylation at *Il4* locus (*Berkley et al., 2013; Makar et al., 2003*). In addition, DNA methylation and histone modification are found to be important for the control of *Ifng* and *Tbx21* expression *(Fang et al., 2022; Friedman et al., 2023; Jones & Chen, 2006)*. Therefore, we next evaluated the contribution of epigenetic modifications to the enhanced IFN-γ production in the absence of IL-27p28. Firstly, we performed bisulfite genomic sequencing on DNA of CD4 SP thymocytes from *Cd11c-cre p28$^{f/f}$* mice and WT littermates. We focused on the nine CpG sites (Figure 3A) most proximal to the *Ifng* transcription start site, among which the -53 CpG has previously been suggested to play a key role in IFN-γ repression in Th2 effector cells (*Jones & Chen, 2006*). DNA methylation was significantly reduced at three CpG sites (-53, -34 and +16 site) of the *Ifng* locus in CD4SP thymocytes from*Cd11c-cre p28$^{f/f}$* mice (Figure 3B). On the contrary, the five CpG sites in the *Il4* promoter region (Figure 3C, D), whose demethylation is associated with high level IL-4 production (*Lee et al., 2002*), showed no difference between cKO and WT CD4SP thymocytes.

As much as histone modifications are concerned, histone H3 lysine 27

trimethylation (H3K27me3) and H3 lysine 9 trimethylation (H3K9me3) are typically associated with repressed *Ifng* and *Tbx21* expression in Th cells, whereas histone H3 lysine 4 trimethylation (H3K4me3) enhances gene expression (*Fang et al., 2022; Friedman et al., 2023*). To evaluate the histone trimethylation modifications at *Ifng*, *Tbx21*, *Il4* and *Gata3* loci in CD4SP thymocytes from WT and *Cd11c-p28*$^{f/f}$ mice, chromatin immunoprecipitation was performed using antibodies against H3K4me3, H3K9me3 and H3K27me3. H3K4me3 was found to be accumulated at *Ifng* and *Tbx21* loci in cKO CD4SP thymocytes, while its level in *Gata3* and *Il4* loci was comparable to that of wild type cells (Figure 3E). On the other hand, neither the occupancy of H3K9me3 and H3K27me3 at *Ifng*, *Tbx21*, *Il4* and *Gata3* loci was altered (Figure 3F, G), nor were the total protein levels of H3K4me3, H3K9me3 H3K27me3 or the mRNA level of enzymes catalyzing the formation of these modifications (Figure 3-figure supplement 1A-C). These results suggest a link between up-regulated *Ifng* and *Tbx21* expression and altered epigenetic modifications in the absence of IL-27p28.

4. Coordinated up-regulation of STAT1-activated genes in CD4SP thymocytes from *Cd11c-p28*$^{f/f}$mice

To better understand the molecular mechanisms underlying the altered functionality, the transcriptional profile of CD4SP thymocytes from *Cd11c-p28*$^{f/f}$ mice was explored by RNA-Seq and compared with that of the WT counterparts. The two sets of differentially expressed genes (DEGs) were subjected to analyses for gene ontology (GO) biological process terms and Kyoto Encyclopedia of Genes and

219 Genomes (KEGG) pathways. The up-regulated DEGs showed significant enrichment
220 in genes related to host defense to viral infection, including interferon response and Jak-
221 STAT signaling (Figure 4A). No meaningful hit, on the other hand, was revealed for the
222 down-regulated gene set (data not shown).

223 Given that STAT1 is a key mediator downstream of IL-27 signaling (*Philips et al.,*
224 *2022*), we were particularly interested in the altered expression of STAT1-regulated
225 genes in the absence of IL-27p28. A previous study by Wan et al. (*Wan et al., 2015*) has
226 compared the transcriptomes of wild-type and STAT1-deficient $CD4^+$ T cells stimulated
227 by IL-21. Using their data (GSE63204), we compiled a list of genes potentially under
228 regulation of STAT1. The DEGs were then examined for overlaps with this gene set.
229 Surprisingly, over 40% of up-regulated DEGs (55 out of 137) fell into the category of
230 STAT1-activated genes, whereas only 2 of them belonged to STAT1-suppressed genes
231 (Figure 4B). To validate the RNA-Seq data, quantitative PCR was carried out for a
232 group of overlapping genes, including *Gm12250, Oasl2, Oas3, Parp14, Ifit3, Usp18,*
233 *Igtp, Irf1, Ifi44, Oas2, Rsad2, Il12r*. As shown in Figure 4C, all these genes showed
234 differential expression between WT and cKO CD4SP thymocytes. To further illustrate
235 modest but coordinate changes in the expression of STAT1-regulated genes, gene set
236 enrichment analysis (GSEA) was performed without imposing an arbitrary fold-change
237 cutoff. Indeed, significant enrichment of STAT1-activated genes was detected in the
238 transcriptome of CD4SP thymocytes from the knockout mice (NES=-2.27, NOM p-
239 val=0, Figure 4D). Therefore, IL-27p28 deficiency resulted in an enhanced STAT1
240 activity.

241 To reveal functionally important connections of the DEGs, protein-protein
242 interaction network was generated using Network Analyst (*Xia et al., 2015*). After
243 removal of isolated and loosely connected nodes, the rest of the proteins encoded by
244 the DEGs were imported into Network Analyst for network construction. As shown in
245 Figure 4E, STAT1 was centrally positioned in the network with the highest degree of
246 interactions. Taken together, these results indicate that IL-27p28 deficiency is strongly
247 associated with an altered transcriptional program featured by enhanced expression of
248 STAT1-activated genes.

249

250 **5. Constitutive activation of STAT1 in CD4SP thymocytes in the absence of IL-**
251 **27p28**

252 The distinct transcriptional signature prompted us to examine the activation status
253 of STAT1 in freshly isolated CD4SP thymocytes from *Cd11c-p28*$^{f/f}$ mice and the WT
254 littermates. Total thymocytes were stained for CD4 and CD8, followed by intracellular
255 staining with antibodies against phosphorylated STATs. Significant levels of STAT1
256 Y701 phosphorylation were observed in cKO but not in WT cells. On the other hand,
257 both cKO and WT cells were stained negative for phosphorylated STAT3 and STAT4
258 (Figure 5A). Phosphorylated and total STAT proteins were also analyzed by Western
259 blotting in purified CD4SP thymocytes, RTEs and naive CD4^{+} T cells. While the total
260 protein of STAT1 was comparable between cKO and WT cells in all populations
261 examined, elevated levels of phosphorylated STAT1 Y701 were constantly detected in
262 cKO cells. Moreover, the phosphorylation of STAT1 Y701 appeared to be

263 developmentally regulated, increasing progressively from CD4SP thymocytes to naive
264 T cells (Figure 5B). Another predominant phosphorylation site in STAT1 is serine 727,
265 which is crucial for maximal STAT1 transcription activity (*Barnholt et al., 2009*). Basal
266 levels of S727 phosphorylation were also observed in CD4SP thymocytes, but with no
267 difference in WT and cKO cells (data not shown). As much as STAT3 and STAT4 were
268 concerned, neither total nor phosphorylated STAT3 and STAT4 were found to be altered
269 with IL-27p28 ablation (Figure 5B), indicating that the impact is specific for STAT1.

270 STAT1 plays an important role in the development of Th1 response by regulating
271 *Tbx21* and *Ifng* expression (*Fang et al., 2022*). To explore the correlation of the
272 increased STAT1 activation with the enhanced T-bet expression and IFN-γ production,
273 we assessed STAT1 binding on the *Tbx21* and *Ifng* loci by ChIP assay. Possibly due to
274 the relatively low abundance of activated STAT1, poor consistency was observed from
275 one experiment to another with freshly isolated CD4SP thymocytes. Therefore, we
276 chose to treat the cells with anti-CD3 and anti-CD28 for 3 days prior to the assay. Under
277 such conditions, STAT1 was found to be markedly accumulated in the promoter and
278 regulatory regions of both *Tbx21* and *Ifng* loci of cKO mice (Figure 5C). Notably, there
279 were strong positive correlations between the levels of STAT1 binding and H3K4me3
280 (Pearson's correlation coefficient for *Ifng* locus $r = 0.917$, $p = 0.010$ and *Tbx21* locus r
281 $= 0.991$, $p < 0.001$, Figure 5D), indicating the implication of STAT1 in the epigenetic
282 modifications of the loci. Together, these data suggest that IL-27p28-medaited signal
283 normally imposes an inhibitory effect on STAT1 activation, which in turn helps the
284 establishment of functional bias against the Th1 lineage.

6. Augmented autoimmune phenotype of *Aire*-deficient mice in the absence of IL-27p28

The physiological significance remains elusive of the bias against the Th1 effector functions for CD4SP thymocytes and RTEs. One hypothesis proposes that it favors the development of peripheral tolerance by avoiding a more inflammatory and potential detrimental response to self-antigens (*Cunningham et al., 2018; Fink & Hendricks, 2011; Hendricks & Fink, 2011*). The disruption of such a bias in *Cd11c-p28*$^{f/f}$ mice provided a good model to test this hypothesis. Flow cytometric analysis of the peripheral T cell compartment demonstrated a significant increase of CD44^{hi}CD62L^{-} activated T cells with a concomitant decrease of CD44^{lo}CD62L^{+} naive T cells in the cKO mice compared to the WT littermates (Figure 6A). Nevertheless, the cKO mice displayed no obvious signs of autoimmunity up to the age of 24-30 weeks when assessed by auto-antibodies against double-strand DNA (Figure 6B) and tissue pathology (Figure 6C). Occasionally, small lymphoid foci were observed in the lung of cKO mice. But the CD4^{+} T cells recovered from the lung tissues displayed a similar cytokine secretion profile to that of WT mice except for the intrinsic augmentation of IFN-γ production (Figure 6D). Therefore, IL-27p28 deficiency alone is insufficient to drive the development of autoimmunity.

We next sought to determine whether IL-27p28 deficiency would affect the autoimmune phonotype in the *Aire*$^{-/-}$ mouse, which are predisposed to developing autoimmunity due to a defect in clonal deletion of autoreactive T cells (*van Laar et al.,*

307 *2022; J. X. Wang et al., 2021*). To this end, *Cd11c-p28*$^{f/f}$ mice were crossed with *Aire*$^{-/-}$
308 mice to generate double knockout mice. Histological examination revealed increased
309 lymphocyte infiltration and more severe structural distortion in the lung and stomach
310 in double knockout mice in comparison to mice deficient for Aire only (Figure 6C). In
311 addition, the double knockout mice exhibited an elevated level of autoantibodies to
312 double-strand DNA, although the difference did not reach a statistical significance
313 (p=0.068) possibly due to the limited sample size (Figure 6B). When CD4^{+} T cells
314 recovered from the lung tissues were analyzed for IFN-γ, IL-4 and IL-17 production,
315 the double knockout mice were virtually indistinguishable from the *Aire*$^{-/-}$ mice, except
316 for increased IFN-γ production (Figure 6D).

317 Immunological anergy constitutes an important mechanism for peripheral
318 tolerance. Two studies have identified a subset of naturally occurring
319 Foxp3^{-}CD44^{hi}CD73^{hi}FR4^{hi} polyclonal CD4^{+} T cells in healthy hosts. They are enriched
320 for self-antigen–specific T cell antigen receptors and represent functionally anergic
321 cells (*ElTanbouly & Noelle, 2021; Kalekar et al., 2016*). We wondered whether the Th1
322 bias induced by IL-27p28 deficiency would affect the generation of the anergic
323 population. As shown in Figure 6E, the CD4^{+}Foxp3^{-}CD44^{hi}CD73^{hi}FR4^{hi} anergic cells
324 were significantly reduced in the double KO mice, which was accompanied by an
325 increase in the CD4^{+}Foxp3^{-}CD44^{hi}CD73^{lo}FR4^{lo} effector/memory cells. Taken together,
326 these data support that the bias against the Th1 lineage in newly generated T cells
327 provides a unique mechanism to render autoreactive cells exquisitely sensitive to
328 tolerance induction.

Discussion

Th2 polarization in adult SP thymocytes and RTEs is believed to be maintained through epigenetic modification at the *Il4* locus. However, the regulation of the opposing cytokine IFN-γ in this context remains unclear. We reported here that thymic DC-derived IL-27p28 played a key role in the establishment of the repressive status of the *Ifng* locus in newly generated $CD4^+$ T cells. As such, the loss of IL-27p28 in DCs endowed these cells with increased capacity of INF-γ production upon TCR engagement. Transcriptome profiling demonstrated coordinated up-regulation of STAT1-activated genes in the absence of IL-27p28. Indeed, enhanced phosphorylation of STAT1 was observed in CD4SP thymocytes from *Cd11c-p28*$^{f/f}$ mice, which was accompanied by the accumulation of STAT1 at the promoter and enhancer regions of *Ifng* and *Tbx21*. Epigenetic analyses indicated reduced DNA methylation at the *Ifng* locus and increased trimethylation of H3K4 at both *Ifng* and *Tbx21* loci in the absence of IL-27p28. Moreover, the H3K4me3 modification was shown to be strongly correlated with STAT1 binding to these loci. These data support a hypothesis that the exposure of developing thymocytes to IL-27p28 induces repressive epigenetic changes at the *Ifng* and *Tbx21* loci, possibly through antagonizing STAT1 activation, ultimately leading to an attenuated IFN-γ response of newly generated CD4SP thymocytes.

The present study revealed a significantly elevated level of phosphorylated STAT1 and up-regulation of a variety of STAT1-regulated genes in CD4SP thymocytes from *Cd11c-p28*$^{f/f}$ mice, indicating that IL-27p28 plays an important role in the fine tuning of STAT1 signaling in the developing thymocytes. As IL-27 is known to activate

multiple STAT proteins, including STAT1, STAT3, STAT4, and STAT5 following engagement of the gp130/IL-27Rα receptor (*Philips et al., 2022*), the hyperactivation of STAT1 in the absence of IL-27p28 is somehow unexpected. We examined the potential impact of IL-27 deficiency on the expression of suppressors of cytokine signaling 3 (SOCS3), which has been shown to have a regulatory role in IL-27 signaling (*Owaki et al., 2006*). Comparable levels of SOCS3 were detected in CD4SP thymocytes and naive $CD4^+$ T cells from *Cd11c-p28*$^{f/f}$ mice and their littermates (Figure 5-figure supplement 1). We also explored the possibility that the constitutive activation of STAT1 might be the secondary effect of enhanced IFN-γ production. Addition of IFN-γ antibodies to the culture of CD4SP thymocytes and naive $CD4^+$ T cells, however, showed no significant effect on phosphorylated STAT1 levels in knockout cells (Figure 5-figure supplement 2A-B). Thus, STAT1 hyperaction is unlikely due to loss of SOCS3 expression or positive feedback of IFN-γ signaling. Of note, it has been previously demonstrated that IL-27p28 on its own can act as a natural antagonist of gp130-mediated signaling triggered by IL-6, IL-11 and IL-27 (*Stumhofer et al., 2010*). Consistent with this finding, Chong et al. reported that IL-27p28 was able to inhibit IL-27-induced Th1 differentiation by reducing the phosphorylation of STAT1 and STAT3 (*Chong et al., 2014*). Therefore, we speculate that IL-27p28 in the thymus may primarily functions to suppress STAT1 activation induced by other cytokines.

A recent study demonstrated that both recombinant murine and human IL-27 induced the expression of antiviral proteins *Oas1*, *Oas2*, *Oas3*, *Oasl1*, and *Oasl2* in epidermal keratinocytes. IL-27 signaling leads to OAS2 expression in a manner

373 dependent on IL27Rα and STAT1, but independent of STAT2. Apart from their antiviral
374 activity, OAS proteins are also involved in cell growth, differentiation, and apoptosis
375 (*Castelli et al., 1997; Huang et al., 2022; Salzberg et al., 1997*). The genomic mutation
376 and methylation of most OAS genes have been shown to alter their expression levels,
377 which is associated with the levels of infiltrated $CD4^+$ T cells and $CD8^+$ T cells in the
378 tumor microenvironment (*Gao et al., 2022*). Secreted OAS2 has also been observed to
379 inhibit CD3 zeta chain expression in T cells (*Dar et al., 2016*). In our current study, we
380 observed an increase in the transcription of *Oasl2, Oas2*, and *Oas3* in CD4SP
381 thymocytes from *Cd11c-p28*$^{f/f}$ mice, indicating that IL-27p28 signaling also involved
382 in the fine-tuning of these OAS protein expressions. Whether these molecules play a
383 role in thymocyte development remains to be clarified.

384 The biased functionality of newly generated $CD4^+$ T cells has been proposed to be
385 important for the induction of peripheral tolerance to self-antigens (*Cunningham et al.,*
386 *2018; Fink & Hendricks, 2011; Hendricks & Fink, 2011*). Despite the much enhanced
387 capacity of IFN-γ production by $CD4^+$ T cells and a significant increase of
388 $CD44^{hi}CD62L^-$ activated T cells, *Cd11c-p28*$^{f/f}$ mice displayed no apparent signs of
389 autoimmunity under steady-state conditions. This is consistent with the result of our
390 previous study in which negative selection was found to proceed normally in *Cd11c-*
391 *p28*$^{f/f}$ mice using the RIP-mOVA and OT-II models (*Tang et al., 2016*). We further
392 interrogated the impact of the disrupted functional bias in *Aire*$^{-/-}$ mice. Aire induces
393 ectopic expression of self-antigens in medullary thymic epithelial cells to mediate
394 negative selection of autoreactive thymocytes. Its mutation causes a rare life-

395 threatening autoimmune disease affecting multiple organs (*van Laar et al., 2022; J. X.*
396 *Wang et al., 2021*). In comparison to *Aire*$^{-/-}$ mice, *Cd11c-p28*$^{f/f}$ *Aire*$^{-/-}$ mice showed
397 elevated levels of double-strand DNA autoantibodies, increased lymphocytes
398 infiltration, and reduced anergic cells. Therefore, although disruption of the functional
399 bias in newly generated T cells is not sufficient to drive autoimmunity, it accelerates
400 disease development in hosts poised for autoimmunity.

401 In further support of a direct link between IL-27 and Aire, a recent study revealed
402 that IL-27 production was inhibited in Aire-overexpressing murine dendritic cells (*Zou*
403 *et al., 2021*). The two subunits IL-27p28 and EBI3 of human IL-27 are usually
404 coordinately expressed in antigen-presenting cells, while mouse IL-27p28 can be
405 secreted independently to inhibit the activities of IL-27 signaling (*Pflanz et al., 2002;*
406 *Stumhofer et al., 2010*). The distinct production profile of IL-27p28 between humans
407 and mice and our finding of the critical role of IL-27p28 in the maintenance of
408 functional bias in newly generated CD4^{+} T cells may explain the much weaker
409 autoimmune phenotype in *Aire*$^{-/-}$ mice than *AIRE*-mutated human subjects. In addition,
410 recent studies have reported elevation of serum IL-27p28 (also known as IL-30) in
411 patients with prostate cancer (*Sorrentino et al., 2019*), psoriasis (*Omar et al., 2021*),
412 and obesity (*Q. Wang et al., 2021*). It would be interesting to explore the involvement
413 of altered functionality of newly generated CD4^{+} T cells under these pathological
414 conditions.

415 Taken together, our data demonstrate that DC-derived IL-27p28 serves as an
416 endogenous inhibitor for STAT1 hyper-activation in developing thymocytes. By

417 regulating DNA and H3K4 methylation levels at the promoter and transcription
418 regulatory regions of *Ifng* and *Tbx21*, it is critically involved in the establishment of the
419 functional bias against IFN-γ production by newly generated $CD4^+$ T cells. Disruption
420 of this mechanism exacerbates autoimmune phenotypes in hosts predisposed for
421 autoimmunity.
422

423 **Materials and methods**

424 **Mice**

425 C57BL/6 mice were obtained from the Vital River Laboratories (Beijing, China).
426 *Cd11c-p28*$^{f/f}$ mice and *Il27ra*$^{-/-}$ mice on C57BL/6 background were kindly provided by
427 Dr. Zhinan Yin from Jinan University (Guangzhou, China). FVB-Tg (Rag2-EGFP)
428 1Mnz/J mice were purchased from Jackson Laboratory (Bar Harbor, ME) and were
429 backcrossed for 10 generations onto the C57BL/6 background (termed as RAG2p-
430 EGFP in this paper). RAG2p-EGFP mice were bred with *Cd11c-p28*$^{f/f}$ mice to generate
431 *Cd11c-p28*$^{f/f}$ RAG2p-EGFP mice. *Aire*$^{-/-}$ mice were generously provided by Yangxin Fu
432 (University of Chicago, IL) and were bred with *Cd11c-p28*$^{f/f}$ mice to generate *Aire*$^{-/-}$
433 *Cd11c-p28*$^{f/f}$ mice. Mice were used at 6-8 weeks of age unless stated otherwise. All the
434 animal procedures were conformed to the Chinese Council on Animal Care Guidelines
435 and the study was approved by the ethics committee of Peking University Health
436 Science Center with an approval number of LA2014178.

437

438 **Antibodies and reagents**

439 PE-Cy7-conjugated anti-mouse CD4 (RM4-5), PE- and APC-conjugated anti-
440 mouse CD8a (53–6.7), APC-conjugated anti-mouse IL-2 (JES6-5H4), PE-Cy7-
441 conjugated anti-mouse TNF-α (MP6-XT22), PE-conjugated anti-mouse Stat1 (pY701)
442 (4a), PerCP-Cy5.5-conjugated anti-mouse Stat3 (pY705) (4/P-STAT3), Alexa Fluor
443 488-conjugated anti-mouse Stat4 (pY693) (38/p-Stat4) were purchased from BD
444 Biosciences (San Diego, CA). PE- and APC-conjugated anti-mouse CD25 (PC61.5)

445 and CD44 (IM7), FITC-conjugated anti-mouse FR4 (eBio12A5), PerCP-eFluor710-
446 conjugated anti-mouse CD73 (eBioTY/11.8), FITC-conjugated anti-mouse IL-4
447 (BVD6-24G2), PE-conjugated anti-mouse IL-17A (eBio17B7), APC-conjugated anti-
448 mouse FOXP3 (3G3), biotin-conjugated anti-mouse CD8a (53–6.7) and anti-phospho-
449 STAT-1(S727) were obtained from eBioscience (Waltham, MA). PE-conjugated anti-
450 mouse IFN-γ (XMG1.2) and PerCP-Cy5.5-conjugated anti-mouse T-bet (4B10) were
451 purchased from BioLegend (San Diego, CA).

452 Functional grade monoclonal antibodies for murine CD3 (145-2C11) and CD28
453 (37.51) and neutralizing anti-IL4 (11B11), neutralizing anti-IFN-γ (clone XMG1.2)
454 were obtained from eBioscience (Waltham, MA). Recombinant murine IL-2, IL-4, IL-
455 6, IL-12 and recombinant human TGF-β1 were purchased from R&D Systems
456 (Abingdon, UK).

457 Anti-phospho-STAT1(Tyr701), anti-STAT1, anti-phospho-STAT3 (Tyr705), anti-
458 STAT3, anti-phospho-STAT4 (Tyr693), anti-STAT4, anti-SOCS3, anti-Actin and HRP-
459 labeled goat-anti-rabbit or anti-mouse IgGs for Western blot assay were purchased from
460 Cell Signaling Technology (Danvers, MA). Phorbol 12-myristate 13-acetate (PMA) and
461 ionomycin were obtained from Sigma-Aldrich.

462

463 **Cell sorting and CD4$^+$ T-cell differentiation *in vitro***

464 To enrich CD4SP thymocytes, CD8$^-$ thymocytes were obtained by negative
465 selection using anti-CD8 (Ly-2) MicroBeads (Miltenyi Biotec). The cells were then
466 stained with fluorescently labeled antibodies to CD4, CD8 and CD44. CD4$^+$SP

467 thymocytes with the phenotype of $GFP^+CD4^+CD8^-CD44^{lo}$ were then sorted. For the
468 isolation of $CD4^+$ RTEs and mature naive $CD4^+$ T cells, $GFP^+CD4^+CD8^-CD25^-NK1.1^-$
469 (RTEs) and $GFP^-CD4^+CD8^-CD25^-CD44^{lo}$ (naive T) cells were sorted from mesenteric
470 lymph nodes. All these cells were sorted to > 99% purity with a FACS Aria II (BD
471 Biosciences, San Diego, CA).

472 For *in vitro* activation, CD4SP thymocytes, RTEs and mature naive T cells were
473 cultured at a density of 2×10^6/mL with plate-coated anti-CD3 (clone 2C11; 2 μg/mL)
474 and soluble anti-CD28 (clone 37N; 1 μg/mL) in RPMl 1640 medium supplemented
475 with 10% fetal bovine serum (Biochrom Ag, Berlin), penicillin, streptomycin and 50
476 μM 2-mercaptoethanol. Conditions for $CD4^+$ T-cell differentiation were as follows: Th0
477 cells, IL-2 (2 ng/mL); Th1 cells, IL-12 (10 ng/mL), IL-2 (2 ng/mL), anti-IL-4 (10
478 μg/mL); Th2 cells, IL-4 (20 ng/mL), IL-2 (2 ng/mL), anti-IFN-γ (10 μg/mL); Th17
479 cells, recombinant human TGFβ1 (10 ng/mL), IL-6 (10 ng/mL), anti-IL-4 (10 μg/mL),
480 anti-IFN-γ (10 μg/mL); and Treg cells, TGFβ1 (1 ng/mL), IL-2 (10 ng/mL), anti-IL-4
481 (10 μg/mL), anti-IFN-γ (10 μg/mL). After 3 days of differentiation, supernatants were
482 collected and cells were subjected to intracellular cytokine staining and flow cytometry
483 analyses.

484

485 **Intracellular staining and flow cytometry**

486 For detection of surface molecules, T cells were labelled with the appropriate
487 fluorescent mAbs on ice for 30 min. For detection of cytoplasmic molecules, T-bet, and
488 FOXP3, T cells were collected, stained with surface molecules, fixed, permeabilized

489 with the Foxp3/Transcription Factor Staining Buffer (eBioscience), and stained with
490 fluorochrome-conjugated mouse antibodies on ice for 30 min. For intracellular cytokine
491 staining, five hours before harvest, T cells were stimulated with PMA (50 ng/mL) plus
492 ionomycin (1 mg/mL) in the presence of a protein transport inhibitor, monensin (2 μM)
493 or BFA (3 μg/mL) (eBioscience). Cells were collected, washed, fixed, permeabilized
494 (FIX AND PERM, Invitrogen) and stained with IFN-γ, IL-4, IL-2, TNF-α, and IL-17
495 antibodies according to the manufacturer's instructions. For detection of
496 phosphorylated STATs, 1×10^7 thymocytes were fixed for 10 min at 37°C with 2%
497 (wt/vol) paraformaldehyde. After fixing, cells were permeabilized for 30 min on ice
498 with 90% (vol/vol) methanol, and stained with the appropriate antibodies. Flow
499 cytometry was conducted on a Galios (Beckman Coulter) and data analysis was
500 performed using Kaluza software.
501

502 **Enzyme-Linked Immunosorbent Assay (ELISA)**

503 Supernatants of *in vitro* cell cultures were obtained at 72 hr. IFN-γ and IL-4
504 production were determined using ELISA kits (BioLegend, San Diego, CA) according
505 to the manufacturer's instructions.

506 For the analysis of anti-dsDNA antibodies, serum was collected from 24-30-week-
507 old *Aire*$^{-/-}$*Cd11c-Cre p28*$^{f/f}$, *Aire*$^{-/-}$, *Cd11c-Cre p28*$^{f/f}$ and WT mice. Nunc MaxiSorp
508 ELISA plates were precoated with dsDNA (100 mg/mL, Sigma, St. Louis, MO) in
509 phosphate-buffered saline (PBS) at 4˚C overnight. Plates were blocked with 5% BSA
510 for 1 hour at 37˚C, then washed and incubated with 1/100 dilutions of mouse sera for 2

511 hours at 37˚C. Plates were washed, and anti-dsDNA antibodies were detected with a
512 1/1000 dilution of alkaline phosphatase–conjugated goat anti-mouse IgG (BioLegend)
513 for 1 hour at 37˚C and developed with a phosphatase substrate for 30 min at 37˚C.
514

515 **Quantitative PCR**

516 RNA was purified from various T cell subsets cultured under Th0 conditions for
517 12 h using Trizol reagent (Invitrogen). cDNA was synthesized using reverse
518 transcription kit (Progema). Quantitative PCR was performed using FastStart Universal
519 SYBR Green Master mix (Roche, Basel, Switzerland) on an iCycler real-time PCR
520 system (Bio-Rad Laboratories, Hemel Hempstead, U.K.), with each sample in triplicate.
521 The quantification was based on delta delta CT calculations and was normalized to β-
522 actin as loading controls. The primers used in the study were listed in Supplementary
523 Table 1.
524

525 **DNA methylation**

526 Bisulfite modification of genomic DNA from FACS purified cells was performed
527 using the EZ DNA methylation kit (Zymo Research). For methylation analysis on *Ifng*
528 gene promoter CpG sites, bisulfite-treated DNA was amplified in semi-nested PCR
529 using primers: 5'-GGTGTGAAGTAAAAGTGTTTTTAGAGAATTTTAT-3' and 5'-
530 CAATAACAACCAAAAACAACCATAAAAAAAAACT-3', then 5'-
531 GGTGTGAAGTAAAAGTGTTTTTAGAGAATTTTAT-3' and 5'-
532 CCATAAAAAAAAACTACAAAACCAAAATACAATA-3'. For methylation analysis

533 on *Il4* gene promoter CpG sites, bisulfite-treated DNA was amplified in PCR using
534 primers: 5-GGATCCACACGGTGCAAAGAGAGACCC-3' and 5′-
535 TCGGCCTTTCAGACTAATCTTATCAGC-3' The PCR products were gel purified
536 and cloned into the pGEM-T vector (Promega; Madison, WI, USA). The inserted PCR
537 fragments of individual clones were sequenced by Tsing KE Biological Technology,
538 Beijing, China. For all samples, 10 reads per CpG site were used to determine the
539 average percentage of methylated CpG.
540

541 **Chromatin immunoprecipitation (ChIP)**

542 ChIP assays were carried out by using Pierce Agarose Chip Kit (Pierce
543 Biotechnology). Briefly, cells were cross-linked for 10 min with 1% formaldehyde and
544 lysed with Nuclease. 10% of the digested chromatin was preserved as input control and
545 the rest of the digested chromatin were incubated with specific antibody or normal IgG
546 (as a control). The purified DNA from immunoprecipitation and the input samples were
547 analyzed by quantitative PCR using primers specific listed in Supplementary Table 1.
548 Data is presented as a percent input of each IP sample relative to input chromatin. The
549 following antibodies were used in ChIP analysis: H3K4me3 (Millipore), H3K27me3
550 (Millipore), H3K9me3 (Abcam), and STAT1 (Cell Signaling Technology).
551

552 **Western blotting**

553 For short term TCR stimulation, CD4SP thymocytes and mature naive T cells were
554 incubated with 2 μg/mL anti-mouse CD3 and 1 μg/mL anti-mouse CD28 on ice for 20

555 min, followed by cross-linking for 10 min at 37°C with 5 μg/mL goat-anti-hamster IgG.
556 Cells were then washed with PBS. Freshly isolated T cells or stimulated T cells were
557 lysed in RIPA buffer for 30 minutes. Whole-cell lysates (5–10 μg per sample) were
558 separated by SDS/PAGE and analyzed by immunoblotting with antibodies to phospho-
559 STAT-1 (Tyr701), phospho-STAT-1 (Ser727), STAT-1, phospho-STAT-3 (Tyr705),
560 STAT-3, phospho-STAT-4 (Tyr693), STAT-4, SOCS3 and Actin. HRP-conjugated anti-
561 Rabbit IgG was used as the detection antibody. The bands were quantified using ImageJ
562 software.
563
564 **RNA-seq**
565 Total RNA was extracted from approximately 2×10^6 CD4SP thymocytes from WT
566 and *Cd11c-p28*$^{f/f}$ mice using Trizol reagent (Invitrogen). Each sample was a mixture of
567 equal amounts of CD4SP thymocytes from three mice. RNA underwent quality control
568 testing using a bionalayser followed by cDNA library preparation. Library construction
569 and sequencing on Illumina HiSEq 2000 were performed by BIOPIC, Peking
570 University.
571
572 **H&E**
573 Organs from 24-30-week-old *Aire*$^{-/-}$*Cd11c-p28*$^{f/f}$ mice, *Aire*$^{-/-}$ mice and WT mice
574 were collected and fixed overnight in 10% formalin, embedded in paraffin, sectioned
575 and stained with hematoxylin and eosin (H&E). The degree of lymphocytic infiltrates

was analyzed in a blinded fashion. In general, 0, 1, 2 and 3 indicate no, mild, moderate, or severe lymphocytic infiltration, respectively.

Statistical analysis

Data are reported as the mean ± Standard deviation (SD). Differences between groups were analyzed by Student's *t* test or two-way Anova (for multiple variant comparisons) using GraphPad Prism software (GraphPad). Throughout the text, figures, and figure legends, the following terminology is used to denote statistical significance: * $P<0.05$, ** $P<0.01$. *** $P<0.001$. NS, no significance.

588 Ashby, K. M., & Hogquist, K. A. (2023). A guide to thymic selection of T cells. *Nat Rev Immunol*.
589 doi:10.1038/s41577-023-00911-8
590 Barnholt, K. E., Kota, R. S., Aung, H. H., & Rutledge, J. C. (2009). Adenosine blocks IFN-gamma-
591 induced phosphorylation of STAT1 on serine 727 to reduce macrophage activation.
592 *Journal of Immunology, 183*(10), 6767-6777. doi:10.4049/jimmunol.0900331
593 Berkley, A. M., Hendricks, D. W., Simmons, K. B., & Fink, P. J. (2013). Recent Thymic Emigrants and
594 Mature Naive T Cells Exhibit Differential DNA Methylation at Key Cytokine Loci. *Journal of*
595 *Immunology, 190*(12), 6180-6186. doi:10.4049/jimmunol.1300181
596 Bhaumik, S., Giffon, T., Bolinger, D., Kirkman, R., Lewis, D. B., Weaver, C. T., & Randolph, D. A. (2013).
597 Retinoic Acid Hypersensitivity Promotes Peripheral Tolerance in Recent Thymic Emigrants.
598 *Journal of Immunology, 190*(6), 2603-2613. doi:10.4049/jimmunol.1200852
599 Cao, Y. X., Doodes, P. D., Glant, T. T., & Finnegan, A. (2008). IL-27 induces a Th1 immune response
600 and susceptibility to experimental arthritis. *Journal of Immunology, 180*(2), 922-930.
601 doi:DOI 10.4049/jimmunol.180.2.922
602 Castelli, J. C., Hassel, B. A., Wood, K. A., Li, X. L., Amemiya, K., Dalakas, M. C., Torrence, P. F., &
603 Youle, R. J. (1997). A study of the interferon antiviral mechanism: apoptosis activation by
604 the 2-5A system. *J Exp Med, 186*(6), 967-972. doi:10.1084/jem.186.6.967
605 Caveney, N. A., Glassman, C. R., Jude, K. M., Tsutsumi, N., & Garcia, K. C. (2022). Structure of the
606 IL-27 quaternary receptor signaling complex. *Elife, 11*. doi:10.7554/eLife.78463
607 Chong, W. P., Horai, R., Mattapallil, M. J., Silver, P. B., Chen, J., Zhou, R., Sergeev, Y., Villasmil, R.,
608 Chan, C. C., & Caspi, R. R. (2014). IL-27p28 inhibits central nervous system autoimmunity
609 by concurrently antagonizing Th1 and Th17 responses. *J Autoimmun, 50*, 12-22.
610 doi:10.1016/j.jaut.2013.08.003
611 Cunningham, C. A., Helm, E. Y., & Fink, P. J. (2018). Reinterpreting recent thymic emigrant function:
612 defective or adaptive? *Curr Opin Immunol, 51*, 1-6. doi:10.1016/j.coi.2017.12.006
613 Dar, A. A., Pradhan, T. N., Kulkarni, D. P., Shah, S. U., Rao, K. V., Chaukar, D. A., D'Cruz, A. K., &
614 Chiplunkar, S. V. (2016). Extracellular 2'5'-oligoadenylate synthetase 2 mediates T-cell
615 receptor CD3-zeta chain down-regulation via caspase-3 activation in oral cancer.
616 *Immunology, 147*(2), 251-264. doi:10.1111/imm.12560
617 Diveu, C., McGeachy, M. J., Boniface, K., Stumhofer, J. S., Sathe, M., Joyce-Shaikh, B., Chen, Y., Tato,
618 C. M., McClanahan, T. K., Malefyt, R. D., Hunter, C. A., Cua, D. J., & Kastelein, R. A. (2009).
619 IL-27 Blocks RORc Expression to Inhibit Lineage Commitment of Th17 Cells. *Journal of*
620 *Immunology, 182*(9), 5748-5756. doi:10.4049/jimmunol.0801162
621 ElTanbouly, M. A., & Noelle, R. J. (2021). Rethinking peripheral T cell tolerance: checkpoints across
622 a T cell's journey. *Nature Reviews Immunology, 21*(4), 257-267. doi:10.1038/s41577-020-
623 00454-2
624 Fang, D., Healy, A., & Zhu, J. (2022). Differential regulation of lineage-determining transcription
625 factor expression in innate lymphoid cell and adaptive T helper cell subsets. *Front*
626 *Immunol, 13*, 1081153. doi:10.3389/fimmu.2022.1081153
627 Fink, P. J., & Hendricks, D. W. (2011). Post-thymic maturation: young T cells assert their individuality.
628 *Nature Reviews Immunology, 11*(8), 544-549. doi:10.1038/nri3028
629 Flores, R. R., Kim, E., Zhou, L., Yang, C., Zhao, J., Gambotto, A., & Robbins, P. D. (2015). IL-Y, a
630 synthetic member of the IL-12 cytokine family, suppresses the development of type 1
631 diabetes in NOD mice. *European Journal of Immunology, 45*(11), 3114-3125.

632 doi:10.1002/eji.201445403
633 Friedman, M. J., Lee, H., Lee, J. Y., & Oh, S. (2023). Transcriptional and Epigenetic Regulation of
634 Context-Dependent Plasticity in T-Helper Lineages. *Immune Netw, 23*(1), e5.
635 doi:10.4110/in.2023.23.e5
636 Gao, L., Ren, R., Shen, J., Hou, J., Ning, J., Feng, Y., Wang, M., Wu, L., Sun, Y., Wang, H., Wang, D.,
637 & Cao, J. (2022). Values of OAS gene family in the expression signature, immune cell
638 infiltration and prognosis of human bladder cancer. *BMC Cancer, 22*(1), 1016.
639 doi:10.1186/s12885-022-10102-8
640 Hamano, S., Himeno, K., Miyazaki, Y., Ishii, K., Yamanaka, A., Takeda, A., Zhang, M., Hisaeda, H.,
641 Mak, T. W., Yoshimura, A., & Yoshida, H. (2003). WSX-1 is required for resistance to
642 infection by regulation of proinflammatory cytokine production. *Immunity, 19*(5), 657-667.
643 doi:Doi 10.1016/S1074-7613(03)00298-X
644 Harker, J. A., Wong, K. A., Dolgoter, A., & Zuniga, E. I. (2015). Cell-Intrinsic gp130 Signaling on CD4
645 T Cells Shapes Long-Lasting Antiviral Immunity. *Journal of Immunology, 195*(3), 1071-
646 1081. doi:10.4049/jimmunol.1402402
647 Hendricks, D. W., & Fink, P. J. (2011). Recent thymic emigrants are biased against the T-helper type
648 1 and toward the T-helper type 2 effector lineage. *Blood, 117*(4), 1239-1249.
649 doi:10.1182/blood-2010-07-299263
650 Huang, Y. Z., Zheng, Y. X., Zhou, Y., Xu, F., Cui, Y. Z., Chen, X. Y., Wang, Z. Y., Yan, B. X., Zheng, M.,
651 & Man, X. Y. (2022). OAS1, OAS2, and OAS3 Contribute to Epidermal Keratinocyte
652 Proliferation by Regulating Cell Cycle and Augmenting IFN-1－Induced Jak1－Signal
653 Transducer and Activator of Transcription 1 Phosphorylation in Psoriasis. *J Invest Dermatol,*
654 *142*(10), 2635-2645 e2639. doi:10.1016/j.jid.2022.02.018
655 Huber, M., Steinwald, V., Guralnik, A., Brüstle, A., Kleemann, P., Rosenplänter, C., Decker, T., &
656 Lohoff, M. (2008). IL-27 inhibits the development of regulatory T cells via STAT3. *Wiener*
657 *Klinische Wochenschrift, 120*, 45-45.
658 Ivashkiv, L. B. (2018). IFNgamma: signalling, epigenetics and roles in immunity, metabolism, disease
659 and cancer immunotherapy. *Nat Rev Immunol, 18*(9), 545-558. doi:10.1038/s41577-018-
660 0029-z
661 Jones, B., & Chen, J. (2006). Inhibition of IFN-gamma transcription by site-specific methylation
662 during T helper cell development. *EMBO J, 25*(11), 2443-2452.
663 doi:10.1038/sj.emboj.7601148
664 Kalekar, L. A., Schmiel, S. E., Nandiwada, S. L., Lam, W. Y., Barsness, L. O., Zhang, N., Stritesky, G. L.,
665 Malhotra, D., Pauken, K. E., Linehan, J. L., O'Sullivan, M. G., Fife, B. T., Hogquist, K. A.,
666 Jenkins, M. K., & Mueller, D. L. (2016). CD4(+) T cell anergy prevents autoimmunity and
667 generates regulatory T cell precursors. *Nat Immunol, 17*(3), 304-314. doi:10.1038/ni.3331
668 Kim, D., Le, H. T., Nguyen, Q. T., Kim, S., Lee, J., & Min, B. (2019). Cutting Edge: IL-27 Attenuates
669 Autoimmune Neuroinflammation via Regulatory T Cell/Lag3-Dependent but IL-10-
670 Independent Mechanisms In Vivo. *Journal of Immunology, 202*(6), 1680-1685.
671 doi:10.4049/jimmunol.1800898
672 Lee, D. U., Agarwal, S., & Rao, A. (2002). Th2 lineage commitment and efficient IL-4 production
673 involves extended demethylation of the IL-4 gene. *Immunity, 16*(5), 649-660.
674 doi:10.1016/s1074-7613(02)00314-x
675 Lin, T. T., Lu, J., Qi, C. Y., Yuan, L., Li, X. L., Xia, L. P., & Shen, H. (2015). Elevated serum level of IL-

676 27 and VEGF in patients with ankylosing spondylitis and associate with disease activity.
677 *Clinical and Experimental Medicine, 15*(2), 227-231. doi:10.1007/s10238-014-0281-x
678 Liu, J. Q., Liu, Z. Z., Zhang, X. J., Shi, Y., Talebian, F., Carl, J. W., Yu, C., Shi, F. D., Whitacre, C. C.,
679 Trgovcich, J., & Bai, X. F. (2012). Increased Th17 and Regulatory T Cell Responses in EBV-
680 Induced Gene 3-Deficient Mice Lead to Marginally Enhanced Development of
681 Autoimmune Encephalomyelitis. *Journal of Immunology, 188*(7), 3099-3106.
682 doi:10.4049/jimmunol.1100106
683 Makar, K. W., Perez-Melgosa, M., Shnyreva, M., Weaver, W. M., Fitzpatrick, D. R., & Wilson, C. B.
684 (2003). Active recruitment of DNA methyltransferases regulates interleukin 4 in
685 thymocytes and T cells. *Nat Immunol, 4*(12), 1183-1190. doi:10.1038/ni1004
686 Mei, Y. W., Lv, Z., Xiong, L. L., Zhang, H. W., Yin, N. L., & Qi, H. B. (2021). The dual role of IL-27 in
687 CD4+T cells. *Molecular Immunology, 138*, 172-180. doi:10.1016/j.molimm.2021.08.001
688 Neufert, C., Becker, C., Wirtz, S., Fantini, M. C., Weigmann, B., Galle, P. R., & Neurath, M. F. (2007).
689 IL-27 controls the development of inducible regulatory T cells and Th17 cells via
690 differential effects on STAT1. *European Journal of Immunology, 37*(7), 1809-1816.
691 doi:10.1002/eji.200636896
692 Nguyen, Q. T., Jang, E., Le, H. T., Kim, S., Kim, D., Dvorina, N., Aronica, M. A., Baldwin, W. M.,
693 Asosingh, K., Comhair, S., & Min, B. (2019). IL-27 targets Foxp3 Tregs to mediate
694 antiinflammatory functions during experimental allergic airway inflammation. *Jci Insight,*
695 *4*(2). doi:10.1172/jci.insight.123216
696 Omar, N. S., Xinxin, L., Jiayi, X., Hussain, S. G., & Biao, P. X. (2021). Serum level of cytokine IL-30 in
697 psoriatic patients and correlation with disease severity. *J Popul Ther Clin Pharmacol, 28*(1),
698 24-33. doi:10.15586/jptcp.2021.v28i1.823
699 Owaki, T., Asakawa, M., Fukai, F., Mizuguchi, J., & Yoshimoto, T. (2006). IL-27 induces Th1
700 differentiation via p38 MAPK/T-bet- and intercellular adhesion molecule-1/LFA-
701 1/ERK1/2-dependent pathways. *Journal of Immunology, 177*(11), 7579-7587.
702 doi:10.4049/jimmunol.177.11.7579
703 Park, J., DeLong, J. H., Knox, J. J., Konradt, C., Wojno, E. D. T., & Hunter, C. A. (2019). Impact of
704 Interleukin-27p28 on T and B Cell Responses during Toxoplasmosis. *Infection and*
705 *Immunity, 87*(12). doi:10.1128/IAI.00455-19
706 Park, Y. J., Ryu, H., Choi, G., Kim, B. S., Hwang, E. S., Kim, H. S., & Chung, Y. (2019). IL-27 confers a
707 protumorigenic activity of regulatory T cells via CD39. *Proceedings of the National*
708 *Academy of Sciences of the United States of America, 116*(8), 3106-3111.
709 doi:10.1073/pnas.1810254116
710 Pflanz, S., Timans, J. C., Cheung, J., Rosales, R., Kanzler, H., Gilbert, J., Hibbert, L., Churakova, T.,
711 Travis, M., Vaisberg, E., Blumenschein, W. M., Mattson, J. D., Wagner, J. L., To, W., Zurawski,
712 S., McClanahan, T. K., Gorman, D. M., Bazan, J. F., de Waal Malefyt, R., Rennick, D., &
713 Kastelein, R. A. (2002). IL-27, a heterodimeric cytokine composed of EBI3 and p28 protein,
714 induces proliferation of naive CD4+ T cells. *Immunity, 16*(6), 779-790. doi:10.1016/s1074-
715 7613(02)00324-2
716 Philips, R. L., Wang, Y., Cheon, H., Kanno, Y., Gadina, M., Sartorelli, V., Horvath, C. M., Darnell, J. E.,
717 Stark, G. R., & O'Shea, J. J. (2022). The JAK-STAT pathway at 30: Much learned, much more
718 to do. *Cell, 185*(21), 3857-3876. doi:10.1016/j.cell.2022.09.023
719 Rose, S., Lichtenheld, M., Foote, M. R., & Adkins, B. (2007). Murine neonatal CD4+ cells are poised

720 for rapid Th2 effector-like function. *Journal of Immunology, 178*(5), 2667-2678.
721 doi:10.4049/jimmunol.178.5.2667
722 Salzberg, S., Hyman, T., Turm, H., Kinar, Y., Schwartz, Y., Nir, U., Lejbkowicz, F., & Huberman, E.
723 (1997). Ectopic expression of 2-5A synthetase in myeloid cells induces growth arrest and
724 facilitates the appearance of a myeloid differentiation marker. *Cancer Res, 57*(13), 2732-
725 2740.
726 Shen, H., Xia, L. P., & Lu, J. (2013). Elevated levels of interleukin-27 and effect on production of
727 interferon-γ and interleukin-17 in patients with Behcet's disease. *Scandinavian Journal of*
728 *Rheumatology, 42*(1), 48-51. doi:10.3109/03009742.2012.704391
729 Sorrentino, C., Yin, Z., Ciummo, S., Lanuti, P., Lu, L. F., Marchisio, M., Bellone, M., & Di Carlo, E.
730 (2019). Targeting Interleukin(IL)-30/IL-27p28 signaling in cancer stem-like cells and host
731 environment synergistically inhibits prostate cancer growth and improves survival. *J*
732 *Immunother Cancer, 7*(1), 201. doi:10.1186/s40425-019-0668-z
733 Stumhofer, J. S., Tait, E. D., Quinn, W. J., Hosken, N., Spudy, B., Goenka, R., Fielding, C. A., O'Hara,
734 A. C., Chen, Y., Jones, M. L., Saris, C. J. M., Rose-John, S., Cua, D. J., Jones, S. A., Elloso, M.
735 M., Grötzinger, J., Cancro, M. P., Levin, S. D., & Hunter, C. A. (2010). A role for IL-27p28 as
736 an antagonist of gp130-mediated signaling. *Nature Immunology, 11*(12), 1119-U1118.
737 doi:10.1038/ni.1957
738 Tang, H., Zhang, J., Sun, X., Qian, X., Zhang, Y., & Jin, R. (2016). Thymic DCs derived IL-27 regulates
739 the final maturation of CD4(+) SP thymocytes. *Sci Rep, 6*, 30448. doi:10.1038/srep30448
740 Tormo, A. J., Meliani, Y., Beaupré, L. A., Sharma, M., Fritz, J. H., Elson, G., Crabé, S., & Gauchat, J. F.
741 (2013). The Composite Cytokine p28/Cytokine-Like Factor 1 Sustains B Cell Proliferation
742 and Promotes Plasma Cell Differentiation. *Journal of Immunology, 191*(4), 1657-1665.
743 doi:10.4049/jimmunol.1201595
744 van Laar, G. G., Hamburg, J. P. V., & Tas, S. W. (2022). Extrathymic AIRE-expressing cells: Friends
745 or foes in autoimmunity and cancer? *Autoimmunity Reviews, 21*(9).
746 doi:10.1016/j.autrev.2022.103141
747 Villarino, A., Hibbert, L., Lieberman, L., Wilson, E., Mak, T., Yoshida, H., Kastelein, R. A., Saris, C., &
748 Hunter, C. A. (2003). The IL-27R (WSX-1) is required to suppress T cell hyperactivity during
749 infection. *Immunity, 19*(5), 645-655. doi:Doi 10.1016/S1074-7613(03)00300-5
750 Wan, C. K., Andraski, A. B., Spolski, R., Li, P., Kazemian, M., Oh, J., Samsel, L., Swanson, P. A., 2nd,
751 McGavern, D. B., Sampaio, E. P., Freeman, A. F., Milner, J. D., Holland, S. M., & Leonard, W.
752 J. (2015). Opposing roles of STAT1 and STAT3 in IL-21 function in CD4+ T cells. *Proc Natl*
753 *Acad Sci U S A, 112*(30), 9394-9399. doi:10.1073/pnas.1511711112
754 Wang, J. X., Lareau, C. A., Bautista, J. L., Gupta, A. R., Sandor, K., Germino, J., Yin, Y., Arvedson, M.
755 P., Reeder, G. C., Cramer, N. T., Xie, F., Ntranos, V., Satpathy, A. T., Anderson, M. S., &
756 Gardner, J. M. (2021). Single-cell multiomics defines tolerogenic extrathymic Aire-
757 expressing populations with unique homology to thymic epithelium. *Science Immunology,*
758 *6*(65). doi:10.1126/sciimmunol.abl5053
759 Wang, Q., Li, D., Cao, G., Shi, Q., Zhu, J., Zhang, M., Cheng, H., Wen, Q., Xu, H., Zhu, L., Zhang, H.,
760 Perry, R. J., Spadaro, O., Yang, Y., He, S., Chen, Y., Wang, B., Li, G., Liu, Z., Yang, C., Wu, X.,
761 Zhou, L., Zhou, Q., Ju, Z., Lu, H., Xin, Y., Yang, X., Wang, C., Liu, Y., Shulman, G. I., Dixit, V.
762 D., Lu, L., Yang, H., Flavell, R. A., & Yin, Z. (2021). IL-27 signalling promotes adipocyte
763 thermogenesis and energy expenditure. *Nature, 600*(7888), 314-318.

764 doi:10.1038/s41586-021-04127-5
765 Xia, J., Gill, E. E., & Hancock, R. E. (2015). NetworkAnalyst for statistical, visual and network-based
766 meta-analysis of gene expression data. *Nat Protoc, 10*(6), 823-844.
767 doi:10.1038/nprot.2015.052
768 Zhang, S., Liang, R. F., Luo, W., Liu, C., Wu, X. L., Gao, Y. A., Hao, J. L., Cao, G. C., Chen, X., Wei, J.,
769 Xia, S. Y., Li, Z., Wen, T., Wu, Y. Y., Zhou, X. L., Wang, P. Y., Zhao, L. Q., Wu, Z. Z., Xiong, S.
770 D., Gao, X. M., Gao, X., Chen, Y. Y., Ge, Q., Tian, Z. G., & Yin, Z. N. (2013). High susceptibility
771 to liver injury in IL-27 p28 conditional knockout mice involves intrinsic interferon-γ
772 dysregulation of CD4 T cells. *Hepatology, 57*(4), 1620-1631. doi:10.1002/hep.26166
773 Zou, X. Y., Wang, S., Zhang, Y., Wang, X. Y., Zhang, R. C., Yang, W., & Li, Y. (2021). AIRE-
774 overexpressing BMDCs suppress TFH cells through ICOSL to prevent and attenuate
775 autoimmune diabetes in NOD mice. *International Immunopharmacology, 99*.
776 doi:10.1016/j.intimp.2021.107979

777

778

Abbreviations

AS, ankylosing spondyliti; BD, behcet disease; ChIP, chromatin immunoprecipitation; cKO, conditional knockout; DC, dendritic cell; DEGs, differentially expressed genes; EAE, experimental autoimmune encephalomyelitis; EBI3, Epstein-Barr virus-induced gene 3; ELISA, Enzyme-Linked Immunosorbent Assay; GO, gene ontology; GSEA, gene set enrichment analysis; H3K4me3, histone H3 lysine 4 trimethylation; H3K27me3, histone H3 lysine 27 trimethylation; H3K9me3, histone H3 lysine 9 trimethylation; IFN-γ, interferon-γ; IL-2, interleukin 2; KEGG, Kyoto Encyclopedia of Genes and Genomes; PBS, phosphate-buffered saline; RTE, recent thymic emigrants; SOCS3, suppressors of cytokine signaling 3; SP, single-positive thymocyte; STAT, signal transducer and activator of transcription; T-bet, T-box transcription factor; Th, T helper; TNF-α, tumor necrosis factor α; WT, wild-type.

Author Contributions

JZ and RJ designed and carried out the study, collected and analyzed the data and drafted the manuscript. JZ and HT performed the phenotype analysis, epigenetic assay and established the mouse model. HMW analyzed the RNA-seq data. XWP performed the cell sorting assay. YZ conceived and designed the study, analyzed the data, and drafted the manuscript. All authors read and approved the final manuscript.

Acknowledgments

We thank Dr. Zhinan Yin from Jinan University (Guangzhou, China) for kindly

provided *Cd11c-cre p28*$^{flox/flox}$ mice and *Il27ra*$^{-/-}$ mice.

Conflicts of Interest

The authors declare no conflict of interest.

Funding

This work was supported by grants from the National Natural Sciences Foundation of China (32230037; 82394412; 32071178; 31872733), National Key Research and Development Program of China (2023YFB3507000).

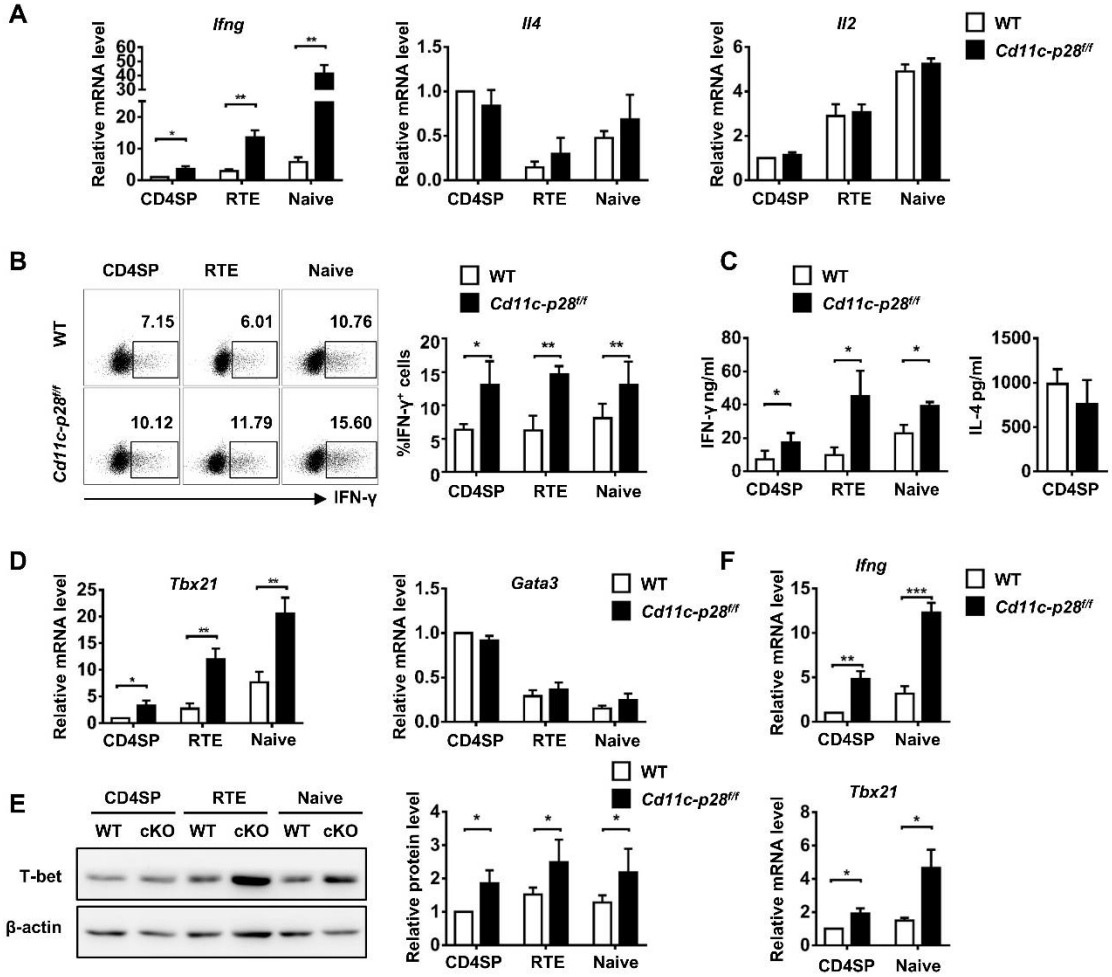

Figure 1. Elevated IFN-γ production and T-bet expression in *Cd11c-p28*$^{f/f}$ mice initiated from CD4SP thymocytes stage.

(A) CD4SP (GFP^{+}CD4^{+}CD8^{-}CD44^{lo}) thymocytes, CD4^{+} RTEs (GFP^{+}CD4^{+}CD8^{-}CD25^{-}CD44^{lo}) and CD4^{+} naive (GFP^{-}CD4^{+}CD8^{-}CD25^{-}CD44^{lo}) T cells were sorted from 6-8-week-old *Cd11c-p28*$^{f/f}$ mice and WT littermates and stimulated with anti-CD3 (2 μg/mL, plate coated) and anti-CD28 (1 μg/mL) for 12 hours. Quantitative PCR analysis was employed to determine the mRNA levels of cytokines, including *Ifng*, *Il4*, and *Il2*. The experiments were conducted four times with duplicates for each sample, and the data are presented as mean ±SD.

(B) Sorted CD4SP thymocytes, CD4^{+} RTEs and CD4^{+} naive T cells from *Cd11c-*

p28$^{f/f}$mice and WT littermates were cultured under Th0 conditions for 3 days. The frequency of IFN-γ-producing CD4^{+} T cells were measured by intracellular staining. Representative dot plots were showed on the left. The statistical data collected from three pairs of mice were shown on the right as mean±SD.

(C) Cells sorted as described in (B) were cultured under Th0 conditions for 3 days, and the concentrations of IFN-γ and IL-4 in the supernatants of CD4SP thymocytes, RTEs, and naive T cells were measured by ELISA. The statistical data collected from three pairs of mice were shown as mean±SD.

(D) Sorted cells were treated as described in (A). The mRNA levels of transcription factors *Tbx21* and *Gata3* were determined by quantitative PCR. The experiments were repeated 4 times with duplicates for each sample and the data are presented as mean±SD.

(E) Western blotting was performed after a 3-day culture under Th0 conditions. The experiments were repeated three times with consistent results. The statistical data showed the relative protein expression levels of T-bet, quantified by densitometry and normalized to β-actin levels (mean±SD).

(F) Freshly sorted cells were dissolved in Trizol. The mRNA levels of *Ifng* and *Tbx21* were determined by quantitative PCR. The experiments were repeated four times with triplicates for each sample and the data are presented as mean±SEM. Statistical differences between groups were determined by the Student's *t*-test. * $P < 0.05$, ** $P < 0.01$, *** $P < 0.001$.

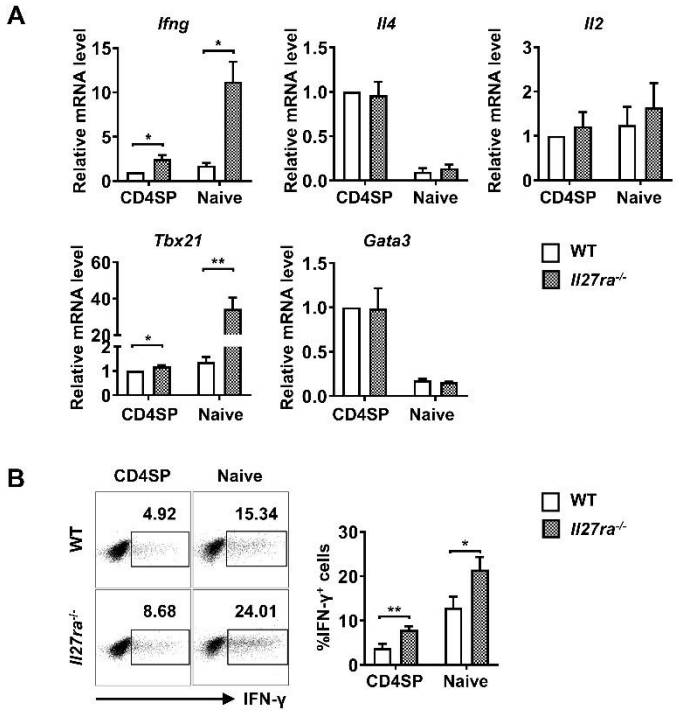

Figure 2. Enhanced IFN-γ production and T-bet expression in *Il27ra*$^{-/-}$ mice initiated from CD4SP thymocytes stage.

(A) CD4SP thymocytes and naive CD4^{+} T cells were isolated from *Il27ra*$^{-/-}$ mice and WT littermates and stimulated with anti-CD3 (2 μg/mL, plate coated) and anti-CD28 (1 μg/mL) for 12 hours. The mRNA levels of cytokines including *Ifng*, *Il4* and *Il2*, and transcription factors *Tbx21* and *Gata3* were determined by quantitative PCR. The experiments were conducted three times with duplicates for each sample and the data are presented as mean±SEM.

(B) CD4SP thymocytes and CD4^{+} naive T cells were cultured under Th0 conditions for 3 days. The frequency of IFN-γ-producing CD4^{+} T cells were determined by intracellular staining. Representative dot plots were showed on the left. The statistical data collected from three pairs of mice were shown on the right as mean±SD. Statistical differences between groups were determined by the Student's *t*-test. * $P< 0.05$, ** $P<$

0.01.

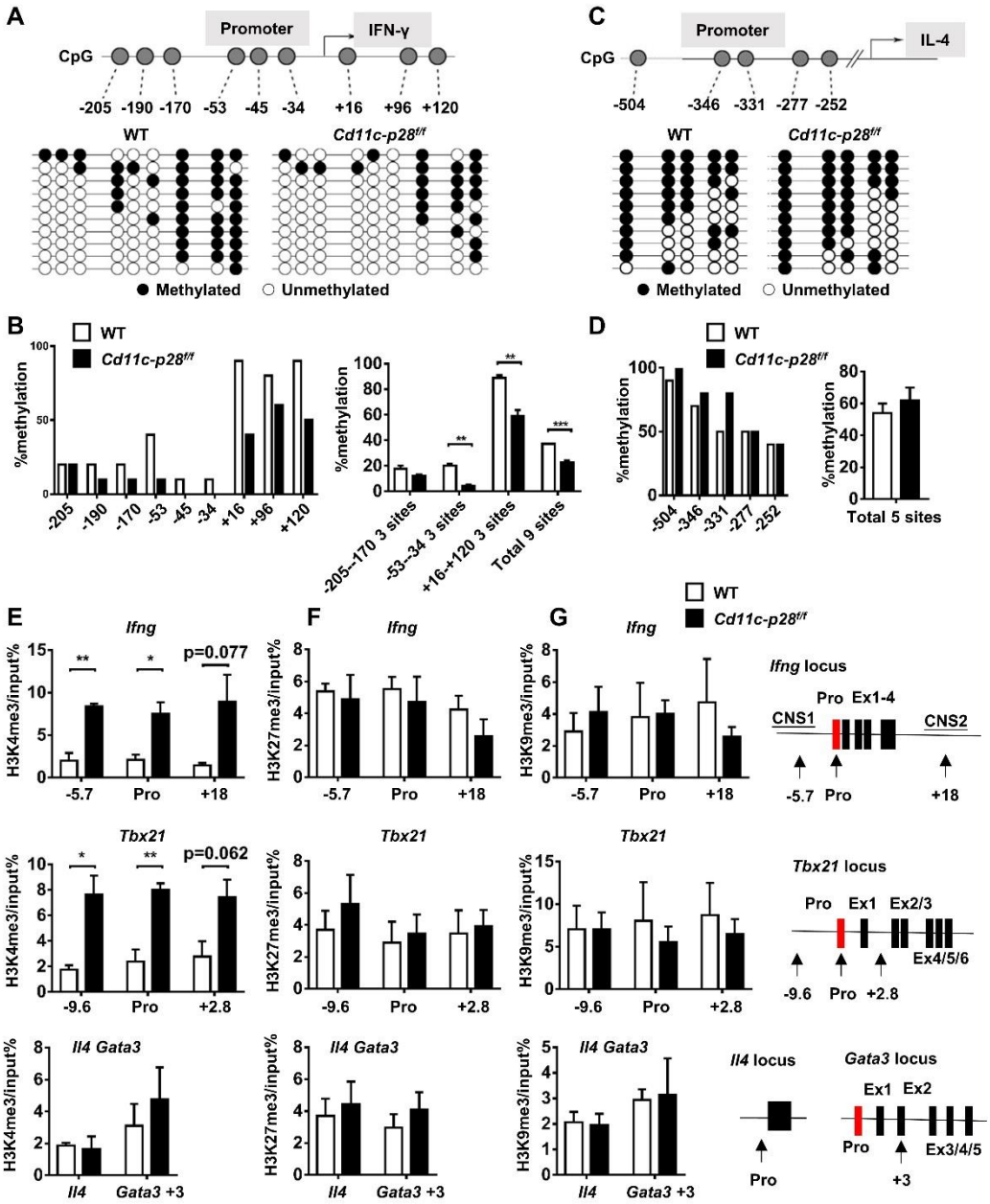

Figure 3. Distinct methylation patterns of DNA and H3K4 at *Ifng* and *Tbx21* promoter regions in CD4SP thymocytes from IL27p28-deficient mice.

(A) DNA methylation analysis of nine sites in the *Ifng* promoter with sodium bisulfite-treated genomic DNA from $GFP^{+}CD4^{+}CD8^{-}CD44^{lo}$ CD4SP thymocytes. Each row represents a cloned and sequenced allele. Analyses included 10 clones from one of the three independent experiments. Filled circles (●) represent methylated cytosine, and open circles (○) the unmethylated residue.

(B) The left panel graphs show the percent of methylation at each individual site from one representative experiment, while the right panel graphs show the average percentage of methylation of three adjacent sites (group1: -205, -190, -170; group2: -53, -45, -34; group3: +16, +96, +120) and all CpG sites from the three independent experiments. The statistical data were shown as mean±SEM.

(C) DNA methylation analysis for five CpG site upstream of the transcription start site of *Il4* with sodium bisulfite-treated genomic DNA from $GFP^{+}CD4^{+}CD8^{-}CD44^{lo}$ CD4SP thymocytes. Each row represents a cloned and sequenced allele. Analyses included 10 clones from the two independent experiments. Filled circles (●) represent methylated cytosine, and open circles (○) the unmethylated residue.

(D) Graphs show the percentage of methylation at each individual site (left panel) or all CpG sites (right panel).

(E-G) Histone trimethylation analysis on freshly isolated CD4SP thymocytes from IL27p28-deficient mice and littermates. ChIP-qPCR was performed using H3K4me3 (E), H3K27me3 (F) and H3K9me3 (G) specific antibodies. Quantitative PCR was conducted using primers specific for the promoters and trans-regulatory regions of *Ifng*, *Tbx21*, *Il4*, and *Gata3*. The experiments were repeated three times with duplicates for each sample and the data are presented as mean±SEM. * $P<0.05$; ** $P<0.01$ determined by Student's *t*-test. Abbreviation: pro., promoter.

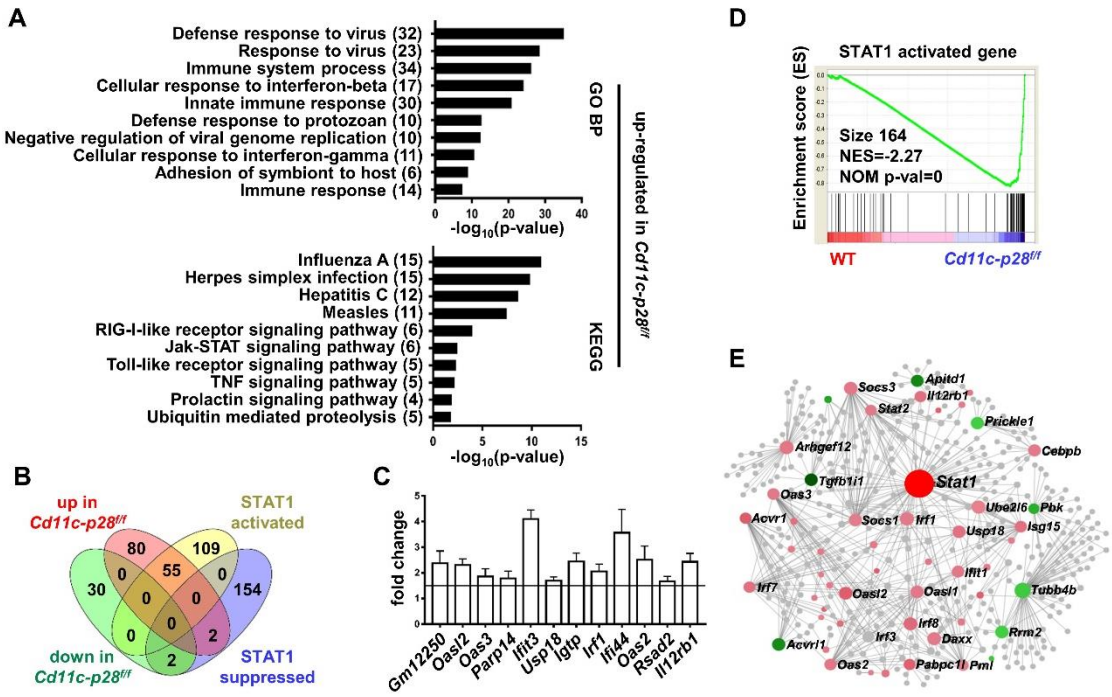

Figure 4. Increased expression of STAT1-activated genes in CD4SP thymcoytes from *Cd11c-p28*$^{f/f}$ mice.

RNA-seq was performed to probe the transcriptome of CD4SP thymcoytes from *Cd11c-p28*$^{f/f}$and WT mice.

(A) The top 10 hits from Gene Ontology (GO) biological process and Kyoto Encyclopedia of Genes and Genomes (KEGG) pathway analyses are shown for Differentially Expressed Genes (DEGs) up-regulated in *Cd11c-p28*$^{f/f}$ mice.

(B) Comparison of genes up- or down-regulated in the absence of IL27p28 (*Cd11c-p28*$^{f/f}$) and those activated or suppressed by STAT1. The numbers of overlapping genes in different categories are indicated.

(C) Validation of the expression levels of representative genes up-regulated by RNA-Seq using quantitative PCR. The experiments were repeated three times with duplicates and data are presented as fold changes in cKO versus WT mice (mean±SEM).

(D) Coordinated upregulation of STAT1-activated genes in CD4SP thymcoytes from *Cd11c-p28*$^{f/f}$ mice revealed by Gene Set Enrichment Analysis (GSEA).

(E) Interaction network of the proteins encoded by DEGs. Nodes represent individual proteins and edges between two nodes represent interactions between proteins. Larger nodes indicate higher degrees of interaction. Red and green nodes represent up-regulated and down-regulated genes, respectively. Gray nodes were not in our DEG datasets but were inserted by Network Analyst as they are connected to the network.

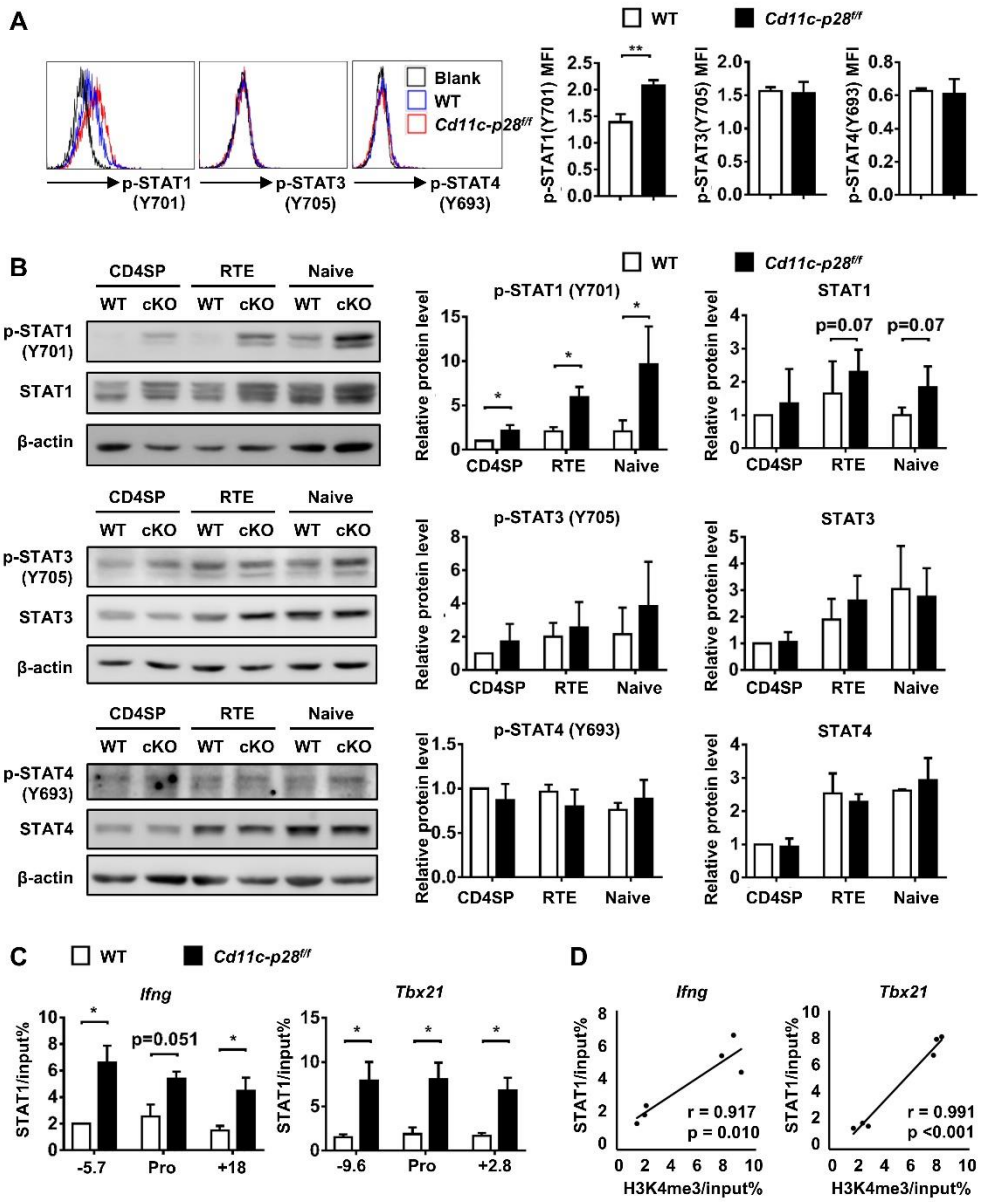

Figure 5. Heightened activation of STAT1 in CD4SP thymocytes from *Cd11c-p28*$^{f/f}$ mice.

(A) Intracellular staining was performed with freshly isolated thymocytes from *Cd11c-p28*$^{f/f}$ mice and WT littermates using antibodies against phosphorylated STAT1 (Y701), STAT3 (Y705) and STAT4 (Y693). Representative histograms are shown for CD4SP thymocytes (*left*). The mean fluorescence intensity (MFI) from three independent experiments are presented as mean±SD (*right*).

(B) Cell lysate was prepared from purified CD4SP thymocytes, $CD4^+$ RTEs and naive $CD4^+$ T cells from WT and *Cd11c-p28*$^{f/f}$ mice. The levels of total and phosphorylated STAT1 (Y701), STAT3 (Y705) and STAT4 (Y693) were examined using Western blotting. The experiments were repeated three times with similar results. Representative blots are shown on the left, and the relative expression levels of phosphorylated and total STATs are presented as mean±SD following quantification by densitometry and normalization to β-actin.

(C) Increased binding of STAT1 onto the promoter and regulatory regions of *Tbx21* and *Ifng* loci.

(D) Correlation of the levels of STAT1 binding and H3K4me3 at the *Tbx21* and *Ifng* loci. * $P<0.05$; ** $P< 0.01$.

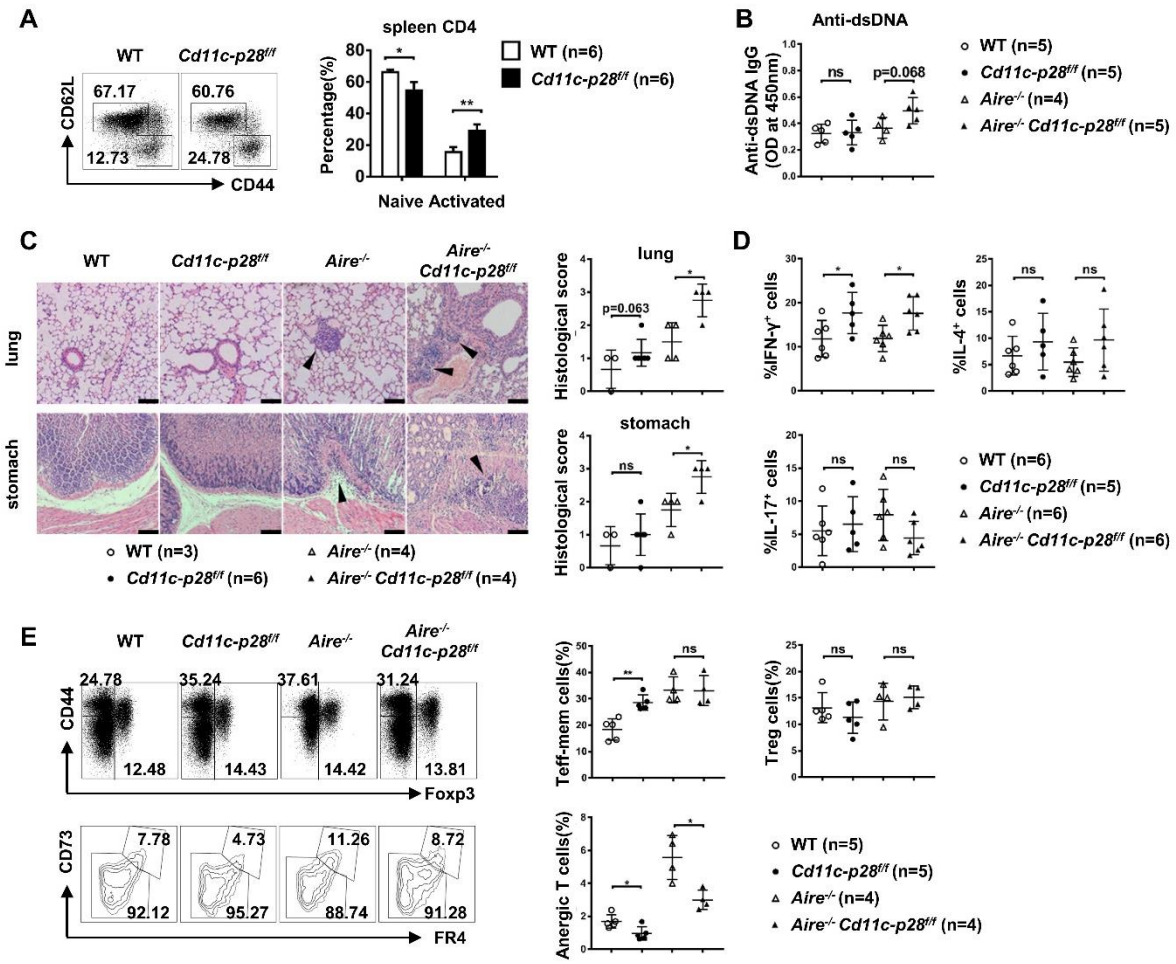

Figure 6. Exacerbated autoimmune responses in *Aire*$^{-/-}$ mice in the absence of IL27p28.

(A) Splenocytes from 6-8 week-old WT (n=6) and *Cd11c-p28*$^{f/f}$ (n=6) mice were analyzed for CD44 and CD62L expression after gating on CD4^{+} T cells. Representative dot plots are shown on the *left*. The percentage of CD44^{lo}CD62L^{+} naive and CD44^{hi}CD62L^{-} activated T cells are presented as mean±SD on the *right*.

(B-D) WT, *Cd11c-p28*$^{f/f}$, *Aire*$^{-/-}$, and *Cd11c-p28*$^{f/f}$ and *Aire*$^{-/-}$ double knockout mice were sacrificed at 24-30 weeks of age and subjected to various analyses. Each symbol represents an individual mouse. The horizontal bars denote the average and SD.

(B) The serum levels of anti-dsDNA antibodies as measured by ELISA.

(C) Representative images of H&E staining (*left*) and histological scores (*right*) of the

lung and stomach. The arrows point to lymphocytic infiltrates. Scale bar equals 100 μm.

(D) The percentage of IFN-γ^+, IL-4^+, and IL-$17A^+$ cells in $CD4^+$ T cells isolated from the lung tissue as determined by intracellular staining following stimulation with PMA/ionomycin.

(E) Splenocytes from 12-week-old mice were stained for the expression of various cellular markers. CD44 and Foxp3 expression was analyzed by gating on $CD4^+$ T cells, and $Foxp3^-CD44^{hi}$ population was further analyzed for CD73 and FR4 staining. The percentage of anergic ($CD4^+Foxp3^-CD44^{hi}CD73^{hi}FR4^{hi}$), effector/memory ($CD4^+Foxp3^-CD44^{hi}CD73^{lo}FR4^{lo}$), and regulatory ($CD4^+Foxp3^+$) T cells are presented on the *right*. Each symbol represents an individual mouse. The horizontal bars denote the average and SD. * $P<0.05$; ** $P<0.01$; ns, not significant.